

Accepted Manuscript

Estimation of in vivo inter-vertebral loading during motion using fluoroscopic and magnetic resonance image informed finite element models

Sahand Zanjani-Pour, Judith R. Meakin, Alex Breen, Alan Breen

PII: S0021-9290(17)30498-0

DOI: <https://doi.org/10.1016/j.jbiomech.2017.09.025>

Reference: BM 8384

To appear in: *Journal of Biomechanics*

Accepted Date: 25 September 2017



Please cite this article as: S. Zanjani-Pour, J.R. Meakin, A. Breen, A. Breen, Estimation of in vivo inter-vertebral loading during motion using fluoroscopic and magnetic resonance image informed finite element models, *Journal of Biomechanics* (2017), doi: <https://doi.org/10.1016/j.jbiomech.2017.09.025>

This is a PDF file of an unedited manuscript that has been accepted for publication. As a service to our customers we are providing this early version of the manuscript. The manuscript will undergo copyediting, typesetting, and review of the resulting proof before it is published in its final form. Please note that during the production process errors may be discovered which could affect the content, and all legal disclaimers that apply to the journal pertain.

Estimation of in vivo inter-vertebral loading during motion using fluoroscopic and magnetic resonance image informed finite element models

Short Communication

Sahand Zanjani-Pour¹, Judith R. Meakin¹, Alex Breen², and Alan Breen³

¹School of Physics and Astronomy, College of Engineering, Mathematics and Physical Sciences, University of Exeter, Exeter, UK

²Institute for Musculoskeletal Research and Clinical Implementation, Anglo-European College of Chiropractic, Bournemouth, UK

³Faculty of Science and Technology, Bournemouth University, Bournemouth, UK

Corresponding author: Judith R. Meakin, Physics Building, Stocker Road, University of Exeter, Exeter, EX4 4QL, UK

Tel. +44 (0) 1392 724109

Email j.r.meakin@exeter.ac.uk

Keywords: Finite element model, Lumbar spine, Fluoroscopy, Magnetic Resonance Imaging

Word count: 2128

Abstract

Finite element (FE) models driven by medical image data can be used to estimate subject-specific spinal biomechanics. This study aimed to combine magnetic resonance (MR) imaging and quantitative fluoroscopy (QF) in subject-specific FE models of upright standing, flexion and extension. Supine MR images of the lumbar spine were acquired from healthy participants using a 0.5 T MR scanner. Nine 3D quasi-static linear FE models of L3 to L5 were created with an elastic nucleus and orthotropic annulus. QF data was acquired from the same participants who performed trunk flexion to 60° and trunk extension to 20°. The displacements and rotations of the vertebrae were calculated and applied to the FE model. Stresses were averaged across the nucleus region and transformed to the disc co-ordinate system (S1 = mediolateral, S2 = anteroposterior, S3 = axial). In upright standing S3 was predicted to be -0.7 ± 0.6 MPa (L3L4) and -0.6 ± 0.5 MPa (L4L5). S3 increased to -2.0 ± 1.3 MPa (L3L4) and -1.2 ± 0.6 MPa (L4L5) in full flexion and to -1.1 ± 0.8 MPa (L3L4) and -0.7 ± 0.5 MPa (L4L5) in full extension. S1 and S2 followed similar patterns; shear was small apart from S23. Disc stresses correlated to disc orientation and wedging. The results demonstrate that MR and QF data can be combined in a participant-specific FE model to investigate spinal biomechanics in vivo and that predicted stresses are within ranges reported in the literature.

Introduction

Determining spinal loads in vivo is essential for understanding normal spine biomechanics and assessing patients with functional impairments. Low back pain is the largest single contributor to disability in many countries across the world (Institute for Health Metrics and Evaluation, 2013) and is regarded as being mechanical in nature in many instances (Borenstein, 2013). Movement patterns are shown to differ between healthy individuals and patients with back pain (Breen and Breen, 2017; Mellor et al., 2014), where an inability to maintain normal movement patterns is thought to be linked through abnormal loading (Mulholland, 2008). Relating movement patterns to the magnitude and sharing of the load, however, is challenging as direct measurement of load in the spine is invasive.

Computational modelling provides a non-invasive method for estimating spinal biomechanics in vivo. Methods include musculoskeletal (MSK) modelling (de Zee et al., 2007; Han et al., 2013) and finite element (FE) analysis which can be used alone e.g. (Dreischarf et al., 2014; Rohlmann et al., 2005) or in combination with MSK modelling e.g. (Shirazi-Adl et al., 2005; Zhu et al., 2013) and allows load distribution between spinal components to be determined. Many models simulate the spine's behaviour by applying forces and/or moments; these may be based on generic values (Dreischarf et al., 2014) or estimated from kinematic measurements using an inverse statics approach (Zhu et al., 2013). An alternative approach is to use medical imaging to observe the motion of the spine and apply this to the model as a displacement. This approach has been investigated previously and demonstrated to be feasible for in-vivo use and to predict disc stresses that are consistent with experimental results (Wang et al., 2013; Wang et al., 2014; Zanjani-Pour et al., 2016).

Our previous work involved the creation of a 2D model using magnetic resonance (MR) images to define both the subject-specific geometry and motion (Zanjani-Pour et al., 2016). The use of MR for determining motion, however, has the disadvantage that that it takes several minutes to set-up and

acquire each image. Quantitative fluoroscopy (QF) provides a method for capturing vertebral motion in-vivo in real time. This technology is emerging in hospitals (Breen et al., 2012), having been shown to have excellent precision and accuracy (Breen et al., 2006).

The aim of this current study was to extend our previous work by developing 3D subject-specific models from MR images and to investigate the incorporation of motion determined from QF to predict spinal loading in upright, flexed and extended postures.

Methods

Participants

Twelve healthy participants were recruited and gave their informed consent to take part in the study. Inclusion criteria were adults aged 21-50 years with no disabling back pain over the previous year. The study received a favourable ethical opinion by the National Research Ethics Service (South West 3, REC reference 10/H0106/65).

Imaging

MR images of the lumbar spine (Figure 1) were acquired from the participants in the supine posture using a 0.5T open bore MR scanner (Paramed Srl., Italy) at the Anglo-European College of Chiropractic (Bournemouth, UK). A volumetric scanning sequence (repetition time, TR = 17 ms, echo time, TE = 8 ms, flip angle = 60°, number of signal averages = 2) provided 3D images comprising voxels of dimension 0.98 x 0.98 x 1.1 mm.

QF data was acquired from the same participants (Figure 1) using a Siemens Arcadis Avantix digital C-arm fluoroscope (Siemens GMBH). The participants performed trunk flexion from upright standing to 60° and trunk extension to 20°; during motion their pelvis was constrained. The central ray was aligned through the L4 disc with exposure factors determined via an automatic exposure device.

Fluoroscopic images were sampled at 15 Hz and analysed by manually placing templates around each vertebral body (performed a total of five times) after which software written in Matlab (V2013, The Mathworks Inc.) was used to automatically track the positions of the vertebrae throughout the image sequences.

The location of the vertebral bodies in the MR and QF image data were used to determine the translation and rotation of the vertebrae from supine to upright, fully flexed (60° flexion), and fully extended (20° extension). Points were manually placed at the corners of the vertebrae L3 to L5 on the MR image at the mid-sagittal plane. These, and the corresponding points on the QF data, were used to determine the vertebral body mid-point (average of the 4 corner points) and vertebral body mid-line (connecting the mid-anterior point (average of the 2 anterior corner points) to the mid-posterior point (average of the 2 posterior corner points)).

The length of the L4 mid-line was used to scale the QF data (which had pixels of unknown size) to the MR data (which had pixels of known size). A translation vector and rotation angle that mapped the location of the vertebral bodies in the MR data onto those in the QF data was then calculated for each vertebral body using the vertebral body mid-points and mid-lines. The error in this mapping process was quantified by calculating the root mean square (RMS) distance between the mapped corner points.

The orientation and wedging of the L3L4 and L4L5 discs were also calculated. Orientation was defined as the angle of the mid-transverse plane of the disc with respect to the horizontal and wedging was defined as the angle between the end-plates of the vertebral bodies; both were calculated from the angles of the lines connecting the two inferior and two superior corner points.

Modelling

Participant-specific 3D FE models of the spine from L3 to L5 were created from the MR data (

Figure 2). The vertebrae and discs (annulus and nucleus) were segmented from the image data and meshed with linear tetrahedral elements using ScanIP and FE+ (Synopsys Ltd., UK). The mesh was refined in the disc regions, producing models with between 70,000 and 100,000 elements.

The models were imported into Abaqus (Dassault Systèmes Simulia Corp.) and material properties assigned. The nucleus was modelled as an isotropic linear elastic material (Young's modulus, $E = 1$ MPa, Poisson's ratio, $\nu = 0.45$)(Williams et al., 2007) and the annulus as an orthotropic linear elastic material. The orthotropic properties of the annulus were calculated from the properties of the fibres ($E = 500$ MPa, $\nu = 0.3$) and matrix ($E = 2.5$ MPA, $\nu = 0.4$)(Williams et al., 2007) using a mixture model and the assumption that the fibre volume fraction was 21% and that the fibres within the annulus lamellae were orientated at 65° to the vertical. The vertebrae were modelled as an isotropic linear elastic material ($E = 100$ MPa, $\nu = 0.2$)(Williams et al., 2007).

The nodes of the mesh in the vertebral bodies (but not the posterior elements) were kinematically coupled to a reference point at the centre of the vertebral body. The translation and rotation of the vertebral bodies, calculated from the image data, were applied to these reference points. The normal and shear stresses in the nucleus were determined and averaged. These were then rotated by the disc orientation angle to determine the stresses in the disc's local coordinate system ($S1 =$ mediolateral, $S2 =$ anteroposterior, $S3 =$ axial).

Data analysis

Differences between postures were assessed using repeated measures analysis of variance followed by post-hoc comparisons with correction for multiple comparisons. Linear and non-linear regression was performed to evaluate the relationship between variables and the strength of the relationship assessed from the coefficient of determination. SPSS (version 23, IBM Corp.) was used for the statistical analyses and statistical significance was taken as a probability less than 0.05.

Results

Nine subject-specific models were created and analysed. Three models could not be created due to difficulty in ascertaining the outline of the vertebrae in the MR data. The RMS error on the mapping procedure ranged from 0.88 mm to 2.2 mm (mean \pm standard deviation: 1.51 ± 0.37 mm).

The orientation and wedging of both discs changed significantly in moving from the upright posture to the flexed posture (Table 1). A change in these variables was found for the motion from the upright to extended posture (Table 1); this was significant for the orientation angle but not the wedging angle.

The normal and shear stresses also changed in moving from the upright posture to both the flexed and extended postures (Figure 3). Many of these changes were statistically significant or exhibited consistent trends (Table 1). No significant differences were found between L3L4 and L4L5 except for shear stress S23 in the upright ($p = 0.037$) and extended posture ($p = 0.002$).

Normal stress was found to have a quadratic relationship with disc orientation (Figure 4a) and a linear relationship with disc wedging (Figure 4c). Shear stress had a linear relationship with both disc orientation (Figure 4b) and disc wedging (Figure 4d). For clarity only the results for S3 and S23 are shown in Figure 4, the results for S1 and S2 were very similar for orientation ($R^2 = 0.34$ and $R^2 = 0.38$) and wedging ($R^2 = 0.27$ and $R^2 = 0.29$) whereas there was little correlation for S12 and S13 with either orientation ($R^2 = 0.18$ and $R^2 = 0.03$) or wedging ($R^2 = 0.12$ and $R^2 = 0.02$).

Discussion

Our previous work on subject-specific modelling used a 2D model where the geometry and motion of the vertebrae were derived from MR images. In the current study we extended this work by creating 3D subject-specific models from MR data and incorporating motion determined from QF data. Stresses in the L3L4 and L4L5 discs were predicted in upright standing, flexion and extension in 9 participants.

The use of a 3D model is an improvement since it is better able to represent the 3D strains present in a real disc and provide a more realistic estimate of stress, pore pressure and disc bulge compared to an equivalent 2D model (Zanjani-Pour, 2016). It also potentially allows the facet joints to be included, opening up the possibility of exploring load sharing between the disc and facet joints; however, in the current study the difficulties in segmenting these from the image data, meant that the facet joints were not analysed. This same issue prevented three subject-specific models from being created. Although the resolution of the MR data was adequate, the low field strength of the scanner meant that the signal to noise ratio was not always sufficient to differentiate the vertebrae from the surrounding tissues.

QF is an imaging method that allows the motion of the spine to be determined in real time. Motion patterns have been shown to differ between healthy controls and patients with low back pain (Breen and Breen, 2017; Mellor et al., 2014) suggesting that the load distribution within the spine may also vary. Although the current study only assessed the end-points of motion, multiple steps in the modelling procedure would allow continuous motion to be modelled. The procedure for determining the translations and rotations of the vertebrae during motion required the QF data to be scaled using the width of L4 measured in the MR data. L4 was chosen because it was at the centre of the image; the scale may have varied slightly away from the centre due to the divergence of the x-ray beam but this effect is anticipated to be small (Breen, 2016). It was also assumed that the vertebral

motion out of the sagittal plane was zero; dual plane fluoroscopy (Wang et al., 2014) provides a way of assessing this but doubles the radiation dose.

The RMS errors in mapping the vertebral corner points in the MR data to those in the QF data were twice those found in our previous work that used MR data alone (Zanjani-Pour et al., 2016). The higher error may have been due to non-uniform scaling or out of plane motion in the QF data but qualitative assessment of the mapped points suggested that the main source of error was the mismatch in selecting corner points in the two different image sets. This may have led to error in the calculated vertebral translations and rotations that affect the predicted disc stresses. Although the magnitude of the vertebral motion error cannot be directly inferred from the magnitude of the mapping error (Shamir and Joskowicz, 2011), we estimate (based on our previous work and an assumption that the translation error scales linearly with the mapping error) that it would be up to 0.6 mm (Zanjani-Pour et al., 2016). However, as the vertebral tracking was performed using rigid templates, the relative error between the upright and flexed or extended postures would be lower, corresponding to the error in the QF tracking of 0.3 mm (Breen et al., 2006).

One of the other limitations in the model is the assumption that the spine was under zero load in the supine posture. This assumption is unlikely to be true since, even though there was an absence of body weight acting on the spine and the participants were imaged in a psoas relaxed posture, there will be some axial load due to passive forces from the ligaments and other muscles. However, measurements in vivo suggest that this would lead to an intradiscal pressure value of around 0.1 MPa (Wilke et al., 1999) which is smaller than the predicted pressures in the upright postures. A second limitation is that the QF data was obtained with the pelvis constrained whereas the experimental results were obtained with an unconstrained pelvis. However, the act of constraining the pelvis has been found to increase paraspinal muscle activity by only 10 % in flexion (Jin and Mirka, 2015).

The disc was modelled as having linear elastic properties from the literature. More sophisticated material models could be used such as in our previous poroelastic model (Zanjani-Pour et al., 2016); however, comparison of predictions from models with different material models shows that although magnitudes differ, the patterns of predicted stress or pressure are similar (Zanjani-Pour, 2016), demonstrating that elastic models can be used to assess inter-subject and inter-posture differences. The subjects in the current study all appeared to have healthy discs but for use in patients it would be desirable to incorporate subject-specific disc properties as these will influence the predicted stresses (Zanjani-Pour et al., 2016). MR parameters such as T1 and T2 relaxation times, magnetization transfer ratio, and diffusion (Cortes et al., 2014; Périé et al., 2006; Recuerda et al., 2012) have previously been shown to relate to disc properties suggesting that they could be used to estimate subject specific properties.

It is difficult to compare the magnitude of the stresses predicted by the model to the existing literature since the amount of flexion and extension differs between our study and many previous studies and because of the model limitations already discussed. However, there are similarities between the results of our model and experimental measurements and previous models in the literature. The greater increase in normal stress from upright standing to flexion compared to upright to extension, for example, is consistent with in-vivo measurements of disc pressure (Sato et al., 1999; Wilke et al., 2001) and other finite element models (Dreischarf et al., 2014; Kuo et al., 2010; Rohlmann et al., 2005) and is consistent with the trunk requiring more muscle forces to provide stability in flexed and extended postures. The change in the direction of the shear stress between L3L4 and L4L5 in upright standing is also consistent with previous models (El-Rich et al., 2004; Galbusera et al., 2014). The relationship between disc normal stress and wedging may seem inconsistent with in-vitro data that suggest compressive loads should be largely independent of

wedging angle (Adams et al., 1994) but can be explained by the fact that wedging and orientation in our study are occurring concurrently rather than as independent variables.

In conclusion, vertebral motion determined from QF data can be incorporated into subject-specific models derived from MR data and the pattern of predicted disc stresses that are consistent with the literature. Additional work is required to minimise mapping errors, incorporate subject-specific material properties, and perform further validation, so that normal and impaired loading and load sharing can be assessed in-vivo.

Acknowledgements

We thank the Chiropractic Research Council, UK for funding this research, Melanie Jones, Superintendent Radiographer at the Anglo-European College of Chiropractic, for acquiring the MR data, and the participants who took part in the study.

Conflict of interest statement

No conflicts of interest.

References

Adams, M.A., McNally, D.S., Chinn, H., Dolan, P., 1994. Posture and the compressive strength of the lumbar spine. *Clin. Biomech.* 9, 5-14.

Borenstein, D., 2013. Mechanical low back pain - a rheumatologist's view. *Nat. Rev. Rheumatol.* 9, 643-653.

Breen, A., 2016. A quantitative fluoroscopic study of the relationship between lumbar inter-vertebral and residual limb/socket kinematics in the coronal plane in adult male unilateral amputees. (Exploring the spine and lower limb kinematics of trans-tibial amputees). Bournemouth University.

Breen, A., Breen, A., 2017. Uneven intervertebral motion sharing is related to disc degeneration and is greater in patients with chronic, non-specific low back pain: an in vivo, cross-sectional cohort comparison of intervertebral dynamics using quantitative fluoroscopy. *Eur. Spine J.*, 1-9.

Breen, A., Muggleton, J., Mellor, F., 2006. An objective spinal motion imaging assessment (OSMIA): reliability, accuracy and exposure data. *BMC Musculoskelet. Disord.* 7, 1-10.

Breen, A.C., Teyhan, D.S., Mellor, F.E., Breen, A.C., Wong, K.W.N., Deitz, A., 2012. Measurement of intervertebral motion using quantitative fluoroscopy: report of an international forum and proposal for using in the assessment of degenerative disc disease in the lumbar spine. *Adv. Orthop.* 2012, 802350.

Cortes, D.H., Magland, J.F., Wright, A.C., Elliott, D.M., 2014. The shear modulus of the nucleus pulposus measured using magnetic resonance elastography: a potential biomarker for intervertebral disc degeneration. *Magn. Reson. Med.* 72, 211-219.

de Zee, M., Hansen, L., Wong, C., Rasmussen, J., Simonsen, E.B., 2007. A generic detailed rigid-body lumbar spine model. *J. Biomech.* 40, 1219-1227.

Dreischarf, M., Zander, T., Shirazi-Adl, A., Puttlitz, C.M., Adam, C.J., Chen, C.S., Goel, V.K., Kiapour, A., Kim, Y.H., Labus, K.M., Little, J.P., Park, W.M., Wang, Y.H., Wilke, H.J., Rohlmann, A., Schmidt, H., 2014. Comparison of eight published static finite element models of the intact lumbar spine: Predictive power of models improves when combined together. *J. Biomech.* 47, 1757-1766.

El-Rich, M., Shirazi-Adl, A., Arjmand, N., 2004. Muscle activity, internal loads, and stability of the human spine in standing postures: combined model and in vivo studies. *Spine* 29, 2633-2642.

Galbusera, F., Brayda-Bruno, M., Costa, F., Wilke, H.-J., 2014. Numerical evaluation of the correlation between the normal variation in the sagittal alignment of the lumbar spine and the spinal loads. *J. Orthop. Res.* 32, 537-544.

Han, K.S., Rohlmann, A., Zander, T., Taylor, W.R., 2013. Lumbar spinal loads vary with body height and weight. *Med. Eng. Phys.* 35, 969-977.

Institute for Health Metrics and Evaluation, 2013. *The Global Burden of Disease: Generating Evidence, Guiding Policy.* IHME, Seattle, WA.

Jin, S., Mirka, G.A., 2015. A systems-level perspective of the biomechanics of the trunk flexion-extension movement: Part I – Normal low back condition. *Int. J. Ind. Ergon.* 46, 7-11.

Kuo, C.-S., Hu, H.-T., Lin, R.-M., Huang, K.-Y., Lin, P.-C., Zhong, Z.-C., Hseih, M.-L., 2010. Biomechanical analysis of the lumbar spine on facet joint force and intradiscal pressure - a finite element study. *BMC Musculoskelet. Disord.* 11, 151.

Mellor, F.E., Thomas, P.W., Thompson, P., Breen, A.C., 2014. Proportional lumbar spine inter-vertebral motion patterns: a comparison of patients with chronic, non-specific low back pain and healthy controls. *Eur. Spine J.* 23, 2059-2067.

Mulholland, R.C., 2008. The myth of lumbar instability: The importance of abnormal loading as a cause of low back pain. *Eur. Spine J.* 17, 619-625.

Périé, D., Iatridis, J.C., Demers, C.N., Goswami, T., Beaudoin, G., Mwale, F., Antoniou, J., 2006. Assessment of compressive modulus, hydraulic permeability and matrix content of trypsin-treated nucleus pulposus using quantitative MRI. *J. Biomech.* 39, 1392-1400.

Recuerda, M., Perie, D., Gilbert, G., Beaudoin, G., 2012. Assessment of mechanical properties of isolated bovine intervertebral discs from multi-parametric magnetic resonance imaging. *BMC Musculoskelet. Disord.* 13, 195.

Rohlmann, A., Zander, T., Bergmann, G., 2005. Comparison of the biomechanical effects of posterior and anterior spine-stabilizing implants. *Eur. Spine J.* 14, 445-453.

Sato, K., Kikuchi, S., Yonezawa, T., 1999. In vivo intradiscal pressure measurement in healthy individuals and in patients with ongoing back problems. *Spine* 24, 2468-2474.

Shamir, R.R., Joskowicz, L., 2011. Geometrical analysis of registration errors in point-based rigid-body registration using invariants. *Med. Image Anal.* 15, 85-95.

Shirazi-Adl, A., El-Rich, M., Pop, D.G., Parnianpour, M., 2005. Spinal muscle forces, internal loads and stability in standing under various postures and loads—application of kinematics-based algorithm. *Eur. Spine J.* 14, 381-392.

Wang, S., Park, W.M., Gadikota, H.R., Miao, J., Kim, Y.H., Wood, K.B., Li, G., 2013. A combined numerical and experimental technique for estimation of the forces and moments in the lumbar intervertebral disc. *Comput Methods Biomech Biomed Engin* 16, 1278-1286.

Wang, S., Park, W.M., Kim, Y.H., Cha, T., Wood, K., Li, G., 2014. In vivo loads in the lumbar L3–4 disc during a weight lifting extension. *Clin. Biomech.* 29, 155-160.

Wilke, H., Neef, P., Hinz, B., Seidel, H., Claes, L., 2001. Intradiscal pressure together with anthropometric data--a data set for the validation of models. *Clin. Biomech.* (Bristol, Avon) 16 Suppl 1, S111-126.

Wilke, H.J., Neef, P., Caimi, M., Hoogland, T., Claes, L.E., 1999. New in vivo measurements of pressure in the intervertebral disc in daily life. *Spine* 24, 755-762.

Williams, J.R., Natarajan, R.N., Andersson, G.B., 2007. Inclusion of regional poroelastic material properties better predicts biomechanical behavior of lumbar discs subjected to dynamic loading. *J. Biomech.* 40, 1981-1987.

Zanjani-Pour, S., 2016. Intervertebral disc stress and pressure in different daily postures: a finite element study., University of Exeter.

Zanjani-Pour, S., Winlove, C.P., Smith, C.W., Meakin, J.R., 2016. Image driven subject-specific finite element models of spinal biomechanics. *J. Biomech.* 49, 919-925.

Zhu, R., Zander, T., Dreischarf, M., Duda, G.N., Rohlmann, A., Schmidt, H., 2013. Considerations when loading spinal finite element models with predicted muscle forces from inverse static analyses. *J. Biomech.* 46, 1376-1378.

Figure captions

Figure 1: MR (mid-sagittal slice) and QF data showing location of templates around vertebral bodies L3 to L5.

Figure 2: Example FE model of L3 to L5.

Figure 3: Normal (a) and shear (b) stresses in L3L4 and L4L5 in upright, 60° of flexion, and 20° of extension. Error bars show 1 standard error about the mean.

Figure 4: Normal and shear stress in the disc as a function of disc orientation and wedging (a) normal stress S_{33} and disc orientation, (b) shear stress S_{23} and disc orientation, (c) normal stress S_{33} and disc wedging, (d) shear stress S_{23} and disc wedging. Plotted data includes values from L3L4 and L4L5 in all three postures.

Table 1. Change in disc angles and stress with posture given as mean and 95% confidence intervals.

		Upright → flexion		Upright → extension	
		Δ (95% CI)	p	Δ (95% CI)	p
Disc orientation (°)	L3L4	30.4 (22.4, 38.5)	0.00	-10.1 (-12.8, -7.5)	0.00
	L4L5	18.8 (12.1, 25.5)	0.00	-9.2 (-11.5, -6.9)	0.00
Disc wedging (°)	L3L4	11.6 (9.0, 14.1)	0.00	-0.6 (-1.4, 0.2)	0.17
	L4L5	11.4 (8.2, 14.7)	0.00	-1.0 (-2.1, 0.1)	0.09
S1 (MPa)	L3L4	-1.09 (-2.2, 0.02)	0.06	-0.35 (-0.64, -0.06)	0.02
	L4L5	-0.57 (-1.04, -0.09)	0.02	-0.07 (-0.27, 0.12)	0.67
S2 (MPa)	L3L4	-1.20 (-2.47, 0.06)	0.06	-0.38 (-0.71, -0.06)	0.02
	L4L5	-0.70 (-1.26, -0.14)	0.02	-0.06 (-0.27, 0.14)	0.76
S3 (MPa)	L3L4	-1.30 (-2.56, -0.04)	0.04	-0.43 (-0.78, -0.07)	0.02
	L4L5	-0.61 (-1.18, -0.04)	0.04	-0.10 (-0.35, 0.16)	0.65
S12 (MPa)	L3L4	0.002 (-0.002, 0.006)	0.54	-0.001 (-0.003, 0.001)	0.20
	L4L5	0.003 (-0.001, 0.007)	0.19	-0.002 (-0.003, 0.000)	0.04
S13 (MPa)	L3L4	-0.002 (-0.005, 0.001)	0.20	0.000 (-0.001, 0.001)	0.64
	L4L5	-0.002 (-0.006, 0.003)	0.67	-0.001 (-0.002, 0.001)	0.63
S23 (MPa)	L3L4	0.229 (0.018, 0.440)	0.03	-0.075 (-0.124, -0.026)	0.01
	L4L5	0.128 (0.035, 0.220)	0.01	-0.015 (-0.064, 0.033)	0.75

Figure 1

[Click here to download Figure: Figure_1_R1.pptx](#)

a



b

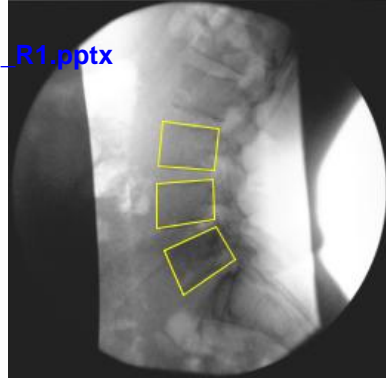


Figure 2

[Click here to download high resolution image](#)

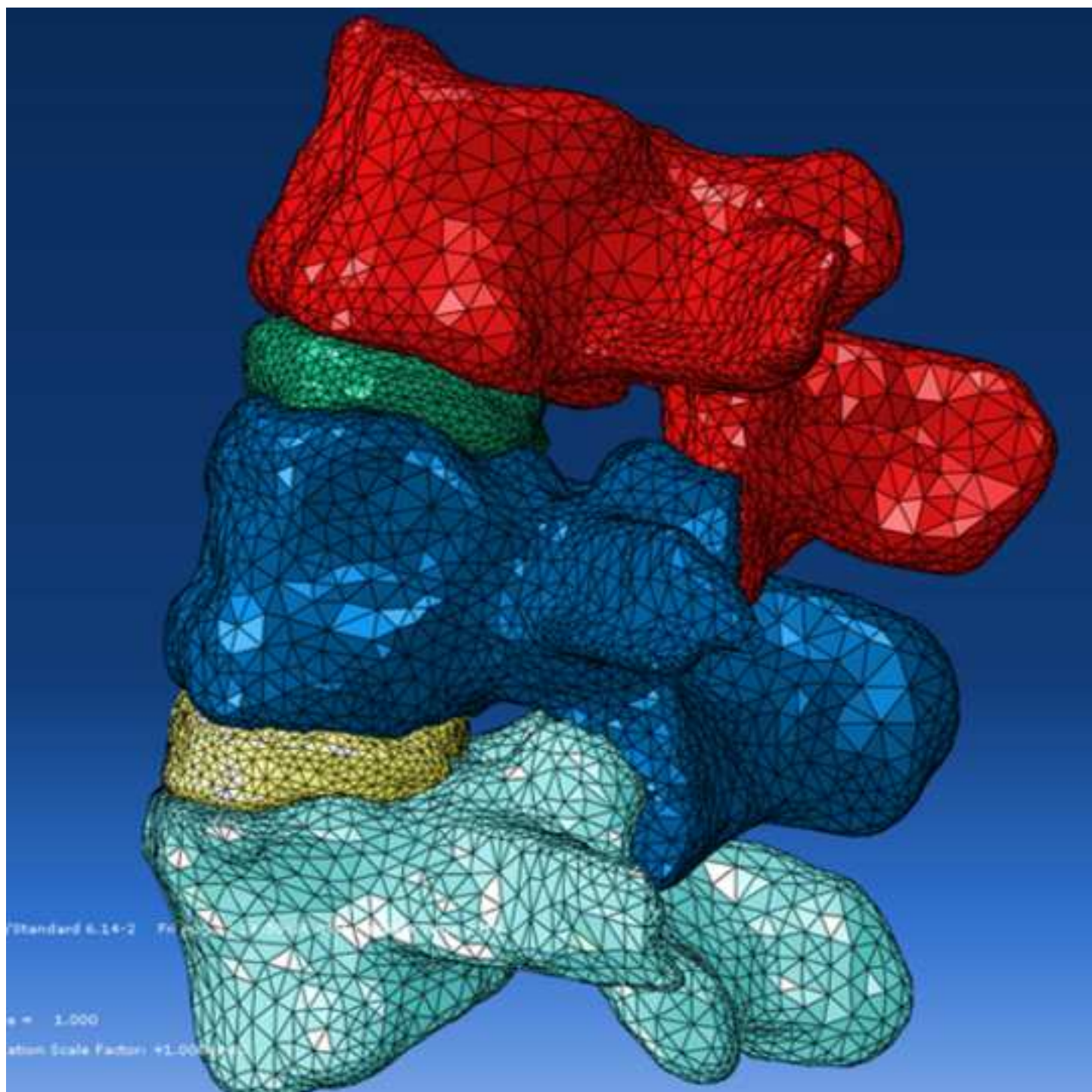


Figure 3a

[Click here to download Figure: Figure3a_R1.pdf](#)

